Water Supply

Water Supply Vol 22 No 4, 3673 doi: 10.2166/ws.2022.012

Defluoridation performance comparison of aluminum hydroxides with different crystalline phases

Wei-Zhuo Gai [a,*], Shi-Hu Zhang[a], Yang Yang[b], Kexi Sun[a], Hong Jia[a] and Zhen-Yan Deng[b]

[a] College of Physics and Electronic Information & Henan Key Laboratory of Electromagnetic Transformation and Detection, Luoyang Normal University, Luoyang 471934, China
[b] Energy Materials & Physics Group, Department of Physics, Shanghai University, Shanghai 200444, China
*Corresponding author. E-mail: gaiweizhuo@126.com

W-ZG, 0000-0001-8815-1919

ABSTRACT

Aluminum hydroxide is an eye-catching and extensively researched adsorbent for fluoride removal and its defluoridation performance is closely related to the preparation method and crystalline phase. In this research, the defluoridation performances of aluminum hydroxides with different crystalline phases are compared and evaluated in terms of fluoride removal capacity, sensitivity to pH values and residual Al contents after defluoridation. It is found that the defluoridation performance of different aluminum hydroxides follows the order of boehmite > bayerite > gibbsite. The fluoride adsorption on aluminum hydroxides follows the pseudo-second-order kinetic model and Langmuir isotherm model, and the maximum defluoridation capacities of boehmite, bayerite and gibbsite are 42.08, 2.97 and 2.74 mg m^{-2}, respectively. The pH values and FTIR analyses reveal that the ligand exchange between fluoride and surface hydroxyl groups is the fluoride removal mechanism. Different aluminum hydroxides have different surface hydroxyl group densities, which results in the different defluoridation capacities. This work provides a new idea to prepare aluminum hydroxide with outstanding defluoridation performance.

Key words: adsorption, aluminum hydroxide, crystalline phase, fluoride removal, surface hydroxyl group

HIGHLIGHTS

- The defluoridation performance of boehmite, bayerite and gibbsite is compared.
- Boehmite exhibits better defluoridation performance than bayerite and gibbsite.
- Fluoride removal mechanism was revealed through pH value and FTIR analyses.
- Adsorption capacity of aluminum hydroxide depends on surface hydroxyl group density.

GRAPHICAL ABSTRACT

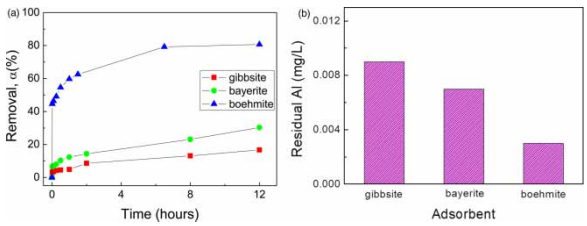

INTRODUCTION

Fluorine is one of the necessary trace elements for human health, and appropriate fluorine can prevent dental caries and maintain the stability of calcium and phosphorus metabolism (Hegde *et al.* 2020). However, both insufficient and excessive fluorine will cause harmful effects on human health. The World Health Organization (WHO) has set 1.5 mg L^{-1} as the guideline of fluoride content in drinking water (Gai & Deng 2021). When the fluoride concentration is lower than 0.5 mg L^{-1}, the incidence rate of dental caries increases. Long-term drinking of high fluoride water (>1.5 mg L^{-1}) can cause a series of fluorosis based

diseases, e.g. dental fluorosis, skeletal fluorosis, joint stiffness, paralysis, thyroid dysfunction and kidney dysfunction (He *et al.* 2020). Tens of million people worldwide are suffering from various degrees of fluorosis due to long-term intake of high fluoride drinking water (Alkurdi *et al.* 2019). Therefore, how to remove the excess fluoride from water is an urgent issue worldwide.

Adsorption is a well-studied and used defluoridation technology due to its simple design, convenient operation and low cost. During the past decades, a variety of adsorbents have been developed, such as natural and modified minerals (García-Sánchez *et al.* 2016), biomass adsorbents (Zhang & Huang 2019), metal oxides and metal hydroxides (Kameda *et al.* 2015), carbon-based adsorbents (Xie *et al.* 2019) and so on. Among these adsorbents, aluminum oxides and hydroxides have the advantages of simple preparation, low cost and strong affinity for fluoride, making them eye catching and extensively researched adsorbents for fluoride removal. Activated alumina is widely used for defluoridation in vast rural areas, but its defluoridation capacity is as low as 1.45 mg g^{-1} (Ghorai & Pant 2004). Some researchers found that the defluoridation performance of alumina could be improved through changing the crystalline phases. For example, the defluoridation capacity of α-Al_2O_3 and γ-Al_2O_3 at 25 °C is 2.73 and 14.0 mg g^{-1}, respectively (Valdivieso *et al.* 2006; Kumar *et al.* 2011). In addition, metal oxides including MgO, MnO_2, CeO_2 and La_2O_3, can be uses as activators to modify alumina and improve defluoridation performance (Dayananda *et al.* 2015; He *et al.* 2019). However, alumina adsorbent has high residual aluminum content after defluoridation, inhibiting its wide application (George *et al.* 2010).

Compared with alumina, aluminum hydroxide has a low residual Al content after defluoridation, making it have more potential than alumina. However, the fluoride removal capacity of commercial aluminum hydroxide is very poor. To enhance the defluoridation efficiency, some methods were developed to prepare aluminum hydroxide adsorbents (Du *et al.* 2014; Sun *et al.* 2016). Shimelis *et al.* (2006) prepared aluminum hydroxide by hydrolysis of aluminum sulfate, and found that the adsorption capacity was 23.7 mg g^{-1}. Gai *et al.* (2015) synthesized aluminum hydroxide by Al-water reaction under ultrasonic field, and demonstrated the maximum defluoridation capacity of 6.78 mg g^{-1}. Jia *et al.* (2015a, 2015b) synthesized bayerite/boehmite adsorbent with 3D feather-like structures through the hydrothermal method, and the adsorbent exhibited excellent adsorption capacity of 56.8 mg g^{-1}. According to the above discussion, aluminum hydroxides prepared by different methods have different defluoridation performances, but the specific reason is unclear. In fact, aluminum hydroxides prepared by different methods have different microstructures and crystalline phases, which may be the reason for their different defluoridation performances. In this work, the impact of crystalline phases on defluoridation efficiency of aluminum hydroxides was systematically analyzed through model experiment, and the related physicochemical mechanism was revealed.

EXPERIMENTAL PROCEDURE

NaF with analytical reagent grade and aluminum hydroxides with three crystalline phases, namely boehmite, bayerite and gibbsite, were used as received in the present experiment. Stock solution with F^- concentration of 1,000 mg L^{-1} was obtained through dissolving an appropriate amount of NaF in deionized water. The aqueous solution with different initial F^- concentration was prepared by diluting the F^- stock solution with deionized water. In each fluoride removal test, 1 g of aluminum hydroxide adsorbent was added into a PTFE beaker containing 250 ml of F^- solution. The suspension was stirred at a speed of 500 rpm using a magnetic stirrer in order to improve the adsorption efficiency. All the adsorption tests were conducted at 25 $\pm$ 1 °C, which was controlled by thermostatic water bath. At a predetermined time, 10 ml of suspension was collected from a beaker using a syringe-driven filter with 0.22 μm polyethersulfone (PES) membrane. After the adsorption test, the adsorbent was recovered by filtering and drying and used for further analysis.

The concentration of fluoride in aqueous solution was measured using an ion meter with a fluoride ion-selective electrode (PF-202-L, Inesa Scientific Instrument Co., Shanghai, China). The fluoride removal efficiency α can be obtained through the following equation:

$$\alpha = \frac{C_0 - C_t}{C_0} \tag{1}$$

where C_0 is the initial F^- concentration, and C_t is the F^- concentration in aqueous solution at time t.

The pH value of F^- solution before and after fluoride removal was determined using a pH meter (PHS-3E, Inesa Scientific Instrument Co., Shanghai, China). The crystalline phases and morphologies of aluminum hydroxides were analyzed using X-ray diffractometry (XRD, D8 Advance, Germany) and scanning electron microscopy (SEM, Sigma 500/VP, Germany), respectively. The functional groups and chemical bonds of adsorbents before and after fluoride removal were analyzed by

Fourier transform infrared spectrometer (FTIR, Avatar 370, USA). Inductively coupled plasma atomic emission spectrometer (ICP-AES, ICAP 6300, USA) was used to analyze the residual Al concentration in solution after defluoridation.

RESULTS AND DISCUSSION

Characterization of aluminum hydroxides

Figure 1 gives the micrographs of aluminum hydroxides with different crystalline phases. It is found that all the aluminum hydroxide particles have irregular shapes, and their particle sizes are non-uniform. The average particle sizes of boehmite, bayerite and gibbsite adsorbents are 17.1, 2.5 and 4.1 μm, respectively.

Figure 2(a) presents the X-ray patterns of aluminum hydroxides with different crystalline phases. For all the aluminum hydroxide adsorbents, only one crystalline phase (boehmite, bayerite and gibbsite) is detected, which validates the high purity of aluminum hydroxides.

Figure 2(b) shows the FTIR spectra of aluminum hydroxides with different crystalline phases. Clearly, aluminum hydroxides with different crystalline phases have obviously different FTIR spectra. The boehmite adsorbent has the bands at 3,302, 3,087, 2,102, 1,631, 1,384, 1,151, 1,074, 742, 613 and 488 cm^{-1}, which are in good agreement with the results of AlOOH in the literature (Wang *et al.* 2009; Zhang *et al.* 2016). The bands at 3,302, 3,087, 1,636, and 1,074 cm^{-1} ascribe to the stretching and bending vibrations of Al-OH, and the bands at 488, 613 and 742 cm^{-1} represent the vibration mode of AlO_6. The bands at 2,102 and 1,384 cm^{-1} correspond to the surface hydroxyl groups (Xu *et al.* 2015). The FTIR spectrum of bayerite is consistent with the standard spectrum of bayerite (Musić *et al.* 1999). The peaks of 3,657, 3,553, 3,467 and 3,424 cm^{-1} belong to the stretching vibrations of hydroxyl groups. For gibbsite, the bands at 3,621, 3,523, 3,463 cm^{-1} result from the OH-stretching

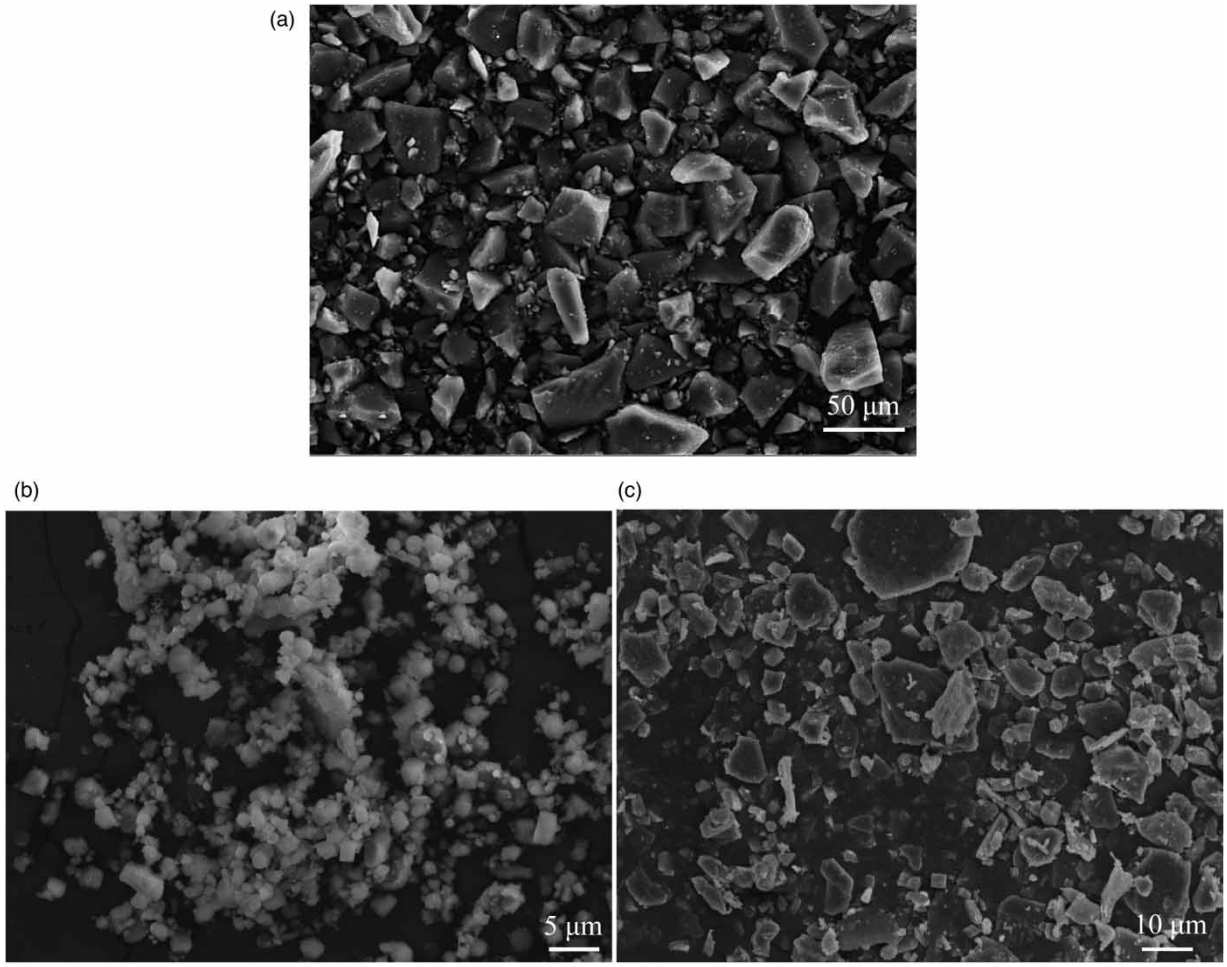

Figure 1 | SEM micrographs of as-received (a) boehmite, (b) bayerite and (c) gibbsite adsorbents.

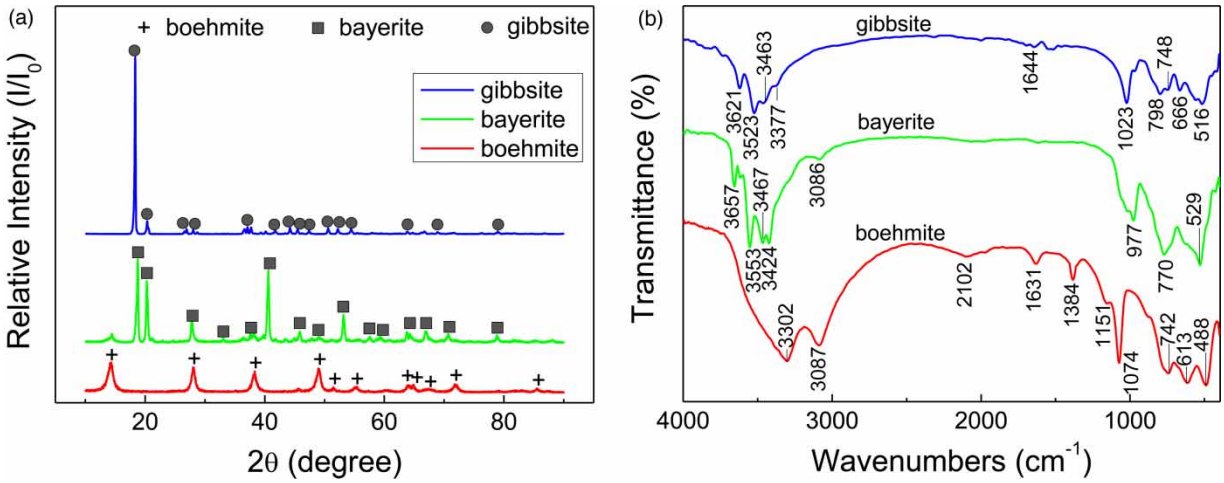

Figure 2 | X-ray patterns (a) and FTIR spectra (b) of as-received boehmite, bayerite and gibbsite adsorbents.

vibrations, the bands at 1,644, 1,023 and 798 cm^{-1} originate from the OH-bending vibrations, and the peaks of 666 and 516 cm^{-1} represent AlO_6 (Alex *et al.* 2014).

Defluoridation performances of aluminum hydroxides

Figure 3(a) shows the fluoride removal performances of aluminum hydroxides with different crystalline phases. Obviously, the crystalline phase of aluminum hydroxide has significant influence on its defluoridation performance. When the initial

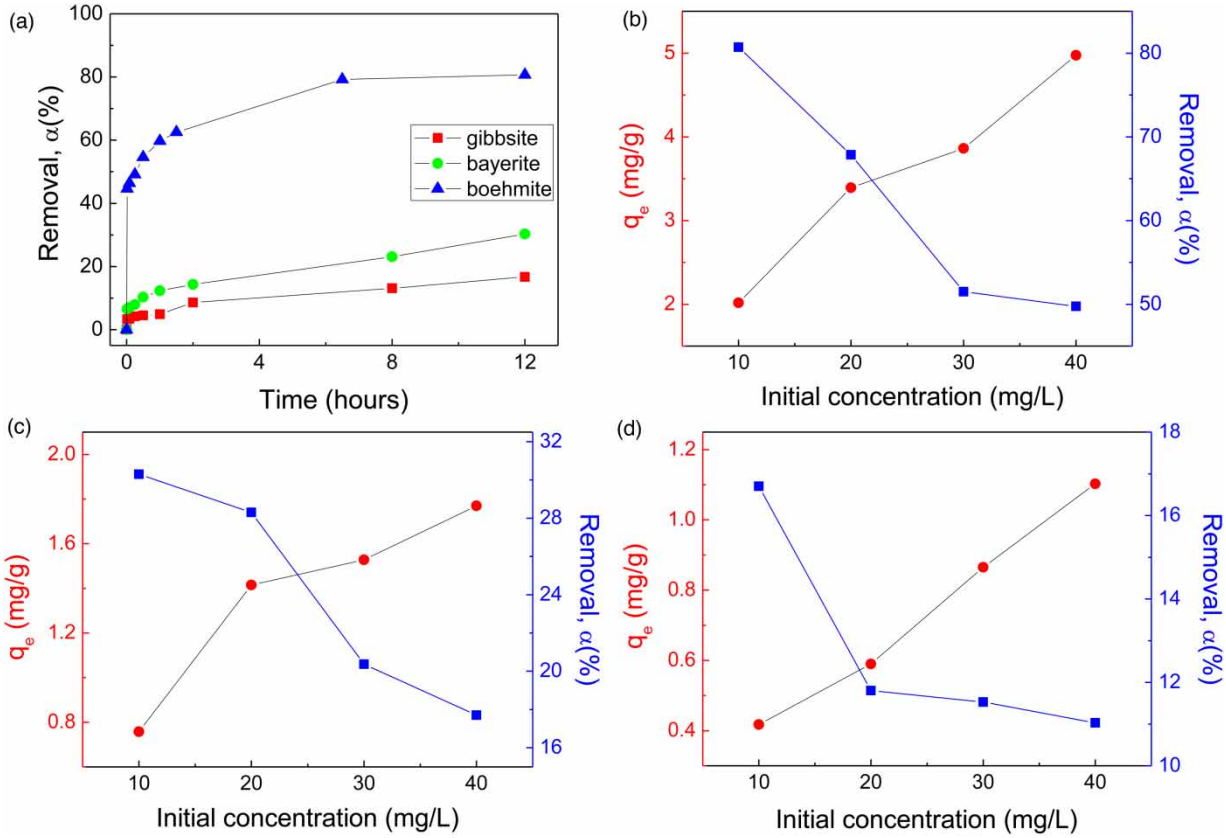

Figure 3 | (a) Fluoride removal from aqueous solution using different aluminum hydroxide adsorbents, where the initial F^- concentration is 10 mg L^{-1}; and the effect of initial F^- concentration on fluoride removal from aqueous solution using (b) boehmite, (c) bayerite and (d) gibbsite adsorbents.

F^- concentration is 10 mg/L, the defluoridation efficiency of boehmite, bayerite and gibbsite is 80.7%, 30.3% and 16.7%, respectively, indicating that the defluoridation performances of aluminum hydroxides with different crystalline phases follow the order of boehmite > bayerite > gibbsite. For boehmite, it can remove >60% fluoride in the first 1.5 h, and reach adsorption equilibrium within 12 h. To further research the defluoridation performance of aluminum hydroxide, the effect of initial F^- concentration on defluoridation efficiency was tested, as shown in Figure 3(b)–3(d). For boehmite, bayerite and gibbsite, the impact trend of initial F^- concentration on defluoridation efficiency is consistent. When increasing the initial F^- concentration, the defluoridation capacity increases, while the defluoridation efficiency decreases. This is reasonable, because the adsorbent cannot provide enough active sites for fluoride adsorption when increasing the initial F^- concentration.

Figure 4 shows the effect of initial pH value on the defluoridation performances of different aluminum hydroxides. Clearly, the defluoridation performance is closely related to the initial pH value. For bayerite and gibbsite adsorbents, the defluoridation capacity remains stable at pH range of 6–9, while it decreases when increasing the pH value from 9 or decreasing the pH value from 6. When the pH value is below 6, some aluminum hydroxide will dissolve, resulting in the reduction of defluoridation capacity. When the pH value is above 9, competitive adsorption between F^- and OH^- occurs, which decreases the defluoridation capacity. For the F^- solution with pH values of 3 and 11, the defluoridation capacities of bayerite and gibbsite are only 0.89 and 0.82 mg g^{-1}, and 0.28 and 0.23 mg g^{-1}, respectively. Compared with bayerite and gibbsite adsorbents, boehmite exhibits excellent defluoridation capacity at a wide pH range of 4 – 10, indicating that boehmite is less sensitive to pH value than bayerite and gibbsite.

Figure 5 shows the effect of adsorption temperature on the defluoridation capacities of different aluminum hydroxides. It was found that temperature has little effect on the defluoridation capacities of different aluminum hydroxides. The defluoridation capacity slightly decreases when increasing the adsorption temperature, indicating that fluoride adsorption on aluminum hydroxide is an exothermic process.

Adsorption kinetics

Understanding of adsorption kinetics is helpful for modeling the adsorption process and designing adsorption-based water treatment systems. The pseudo-first-order and pseudo-second-order models were used to analyze the experimental data for F^- adsorption on aluminum hydroxide according to the following equations (Jia *et al.* 2015a, 2015b):

Pseudo-first-order: $$q_t = q_e(1 - e^{-k_1 t}) \quad (2)$$

Pseudo-second-order: $$q_t = \frac{q_e^2 k_2 t}{1 + k_2 q_e t} \quad (3)$$

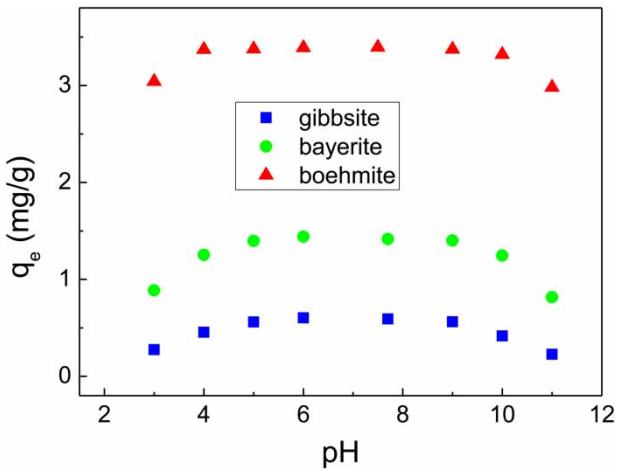

Figure 4 | Fluoride removal from F- solution with different pH values using different aluminum hydroxide adsorbents, where the initial F^- concentration is 20 mg L^{-1} and the temperature is 25 °C.

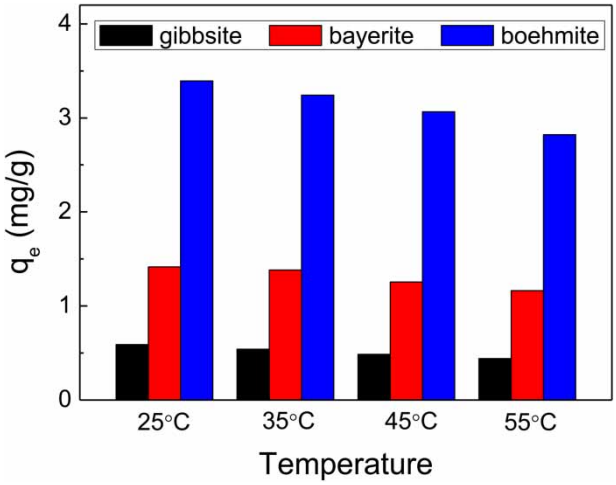

Figure 5 | Fluoride removal from F^- solution at different temperatures using different aluminum hydroxide adsorbents, where the initial F^- concentration is 20 mg L^{-1}.

where q_t and q_e are the amount of fluoride adsorbed on adsorbent (mg g^{-1}) at time t and equilibrium, respectively, q_{max} is the maximum adsorption capacity, K_L is the binding energy constant, k_1 and k_2 are the rate constants for the pseudo-first-order and pseudo-second-order kinetics.

Figure 6 shows the pseudo-first-order and pseudo-second-order nonlinear kinetic plots for the fluoride adsorption on different aluminum hydroxides, and the corresponding parameters are given in Table 1. According to the correlation coefficient

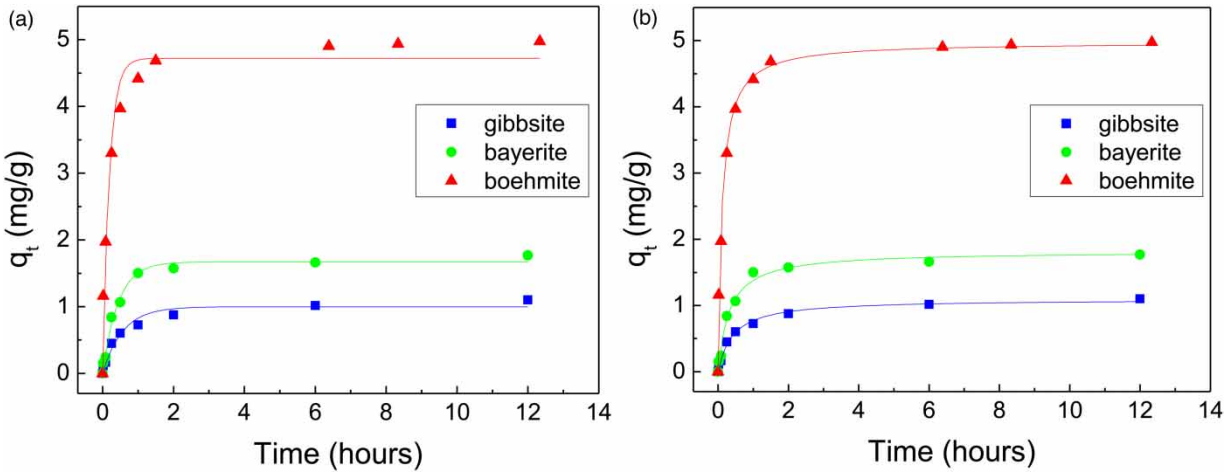

Figure 6 | Nonlinear pseudo-first-order kinetic fit (a) and nonlinear pseudo-second-order kinetic fit (b) for fluoride removal from aqueous solution using different aluminum hydroxide adsorbents, where the initial fluoride concentration is 40 mg L^{-1} and the temperature is 25 °C.

Table 1 | Kinetic parameters of pseudo-first-order and pseudo-second-order models obtained by the nonlinear regression approach for fluoride adsorption on aluminum hydroxides

		Pseudo-first-order			Pseudo-second-order		
Adsorbents	$q_{e(exp)}$ (mg g^{-1})	q_e (mg g^{-1})	k_1 (h^{-1})	R^2	q_e (mg g^{-1})	k_2 (g mg^{-1} h^{-1})	R^2
Gibbsite	1.10	1.00	1.761	0.959	1.10	2.169	0.990
Bayerite	1.77	1.67	2.294	0.986	1.82	1.726	0.987
Boehmite	4.98	4.72	5.288	0.957	4.98	1.734	0.987

(R^2), the adsorption data fits better with the pseudo-second-order model than the pseudo-first-order model, implying that the adsorption of fluoride on aluminum hydroxide follows second-order adsorption.

Adsorption isotherm

In order to determine the adsorption capacity of aluminum hydroxides, the adsorption isotherms of different aluminum hydroxides were analyzed. As shown in Figure 7, both Langmuir and Freundlich isotherm models were used to fit the defluoridation data according to the following equations (Srivastav *et al.* 2013):

$$\text{Langmuir:} \quad \frac{1}{q_e} = \left(\frac{1}{q_{\max} K_L}\right)\frac{1}{C_e} + \frac{1}{q_{\max}} \tag{4}$$

$$\text{Freundlich:} \quad \log q_e = \log K_F + \frac{1}{n}\log C_e \tag{5}$$

where C_e and q_e are the F^- concentration and adsorption capacity at equilibrium, respectively, $q_{\max}$ is the maximum adsorption capacity, K_L is the binding energy constant, K_F and n are the Freundlich constants corresponding to adsorption capacity and favorable degree of adsorption. Table 2 gives the isotherm model parameters for F^- adsorption by different aluminum hydroxides. According to the correlation coefficient (R^2), the adsorption data fits better with the Langmuir model than the Freundlich model, implying that the adsorption of fluoride on aluminum hydroxide is monolayer adsorption. Based on Langmuir model, the maximum adsorption capacities of boehmite, bayerite and gibbsite are 5.05, 2.97 and 1.67 mg g^{-1}, which further confirms that the defluoridation performance of different aluminum hydroxides follows the order of boehmite > bayerite > gibbsite.

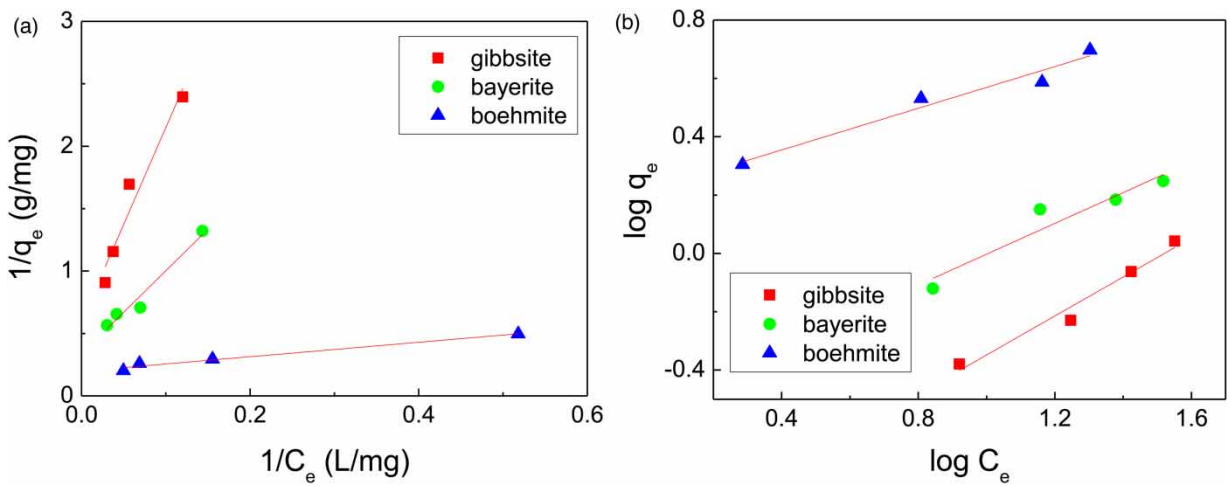

Figure 7 | Langmuir (a) and Freundlich (b) adsorption isotherms for fluoride removal from aqueous solution using different aluminum hydroxide adsorbents.

Table 2 | Isotherm parameters of Langmuir and Freundlich models for fluoride adsorption by aluminum hydroxides

	Langmuir			Freundlich		
Adsorbents	q_{max} (mg g^{-1})	k_L (L mg^{-1})	R^2	k_F	n	R^2
Gibbsite	1.67	0.0385	0.921	0.0964	1.497	0.956
Bayerite	2.97	0.0506	0.950	0.2947	1.894	0.869
Boehmite	5.05	0.3414	0.965	1.6286	2.799	0.945

Residual Al after defluoridation

As is known, some aluminum can leach into water in the defluoridation process using Al-based materials as adsorbents. Al is a potential neurotoxin, and WHO has set 0.2 mg L^{-1} as the concentration limit of Al in drinking water (George *et al.* 2010). Long-term drinking water with excessive Al may enhance the risk for the development of Alzheimer's disease in humans (Rondeau *et al.* 2000). Therefore, it is necessary and meaningful to analyze the residual Al after defluoridation when evaluating the defluoridation performance of aluminum hydroxides. Figure 8 illustrates the residual Al concentration of aqueous solution after defluoridation using aluminum hydroxides with different crystalline phases. As can be seen, the residual Al concentrations after defluoridation by gibbsite, bayerite and boehmite are 0.009, 0.007 and 0.003 mg L^{-1}, respectively, which are far below the WHO limit. This indicates that all three aluminum hydroxides can be used for fluoride removal.

Comparison of defluoridation performance

To comprehensively compare the defluoridation performance of aluminum hydroxides with different crystalline phases, Table 3 summarizes the fluoride removal capacities and residual Al contents of different aluminum hydroxides. As is known, the adsorption capacity of an adsorbent is closely related to the specific surface area. To get rid of the impact of surface area, the defluoridation capacity per unit area ($q_{max,s}$) is also calculated and given in Table 3. Boehmite, bayerite and gibbsite have the defluoridation capacity per unit area of 42.08, 2.97 and 2.74 mg m^{-2}. Based on the defluoridation capacity and residual Al content, it can be inferred that the defluoridation performance of different aluminum hydroxides follows the order of boehmite > bayerite > gibbsite.

In order to further assess the fluoride removal performances of different aluminum hydroxides, the adsorption capacities of aluminum hydroxides from present study were compared with other Al-based adsorbents, as shown in Table 4. It can be seen that boehmite exhibits excellent defluoridation capacity and fast adsorption rate, indicating that boehmite has more potential than bayerite and gibbsite for fluoride removal.

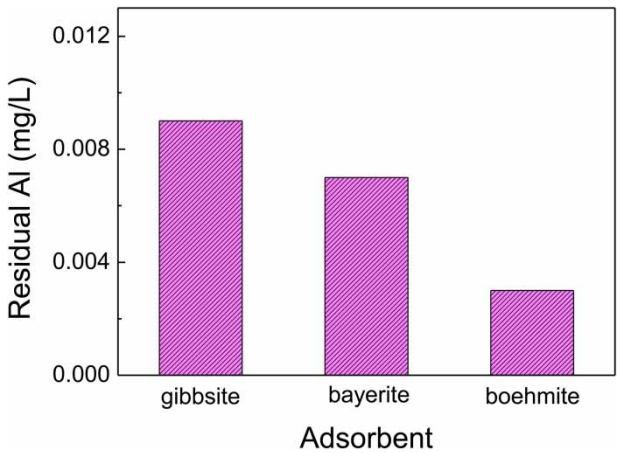

Figure 8 | Residual Al concentration of aqueous solution after fluoride removal using different adsorbents, where the initial F^- concentration is 20 mg L^{-1}.

Table 3 | Defluoridation performances of aluminum hydroxides with different crystalline phases

Adsorbents	Particle size (μm)	Surface area (m^2 g^{-1})	Residual Al (mg L^{-1})	$q^a_{max,m}$ (mg g^{-1})	$q^a_{max,s}$ (mg m^{-2})
Boehmite	17.1	0.12	0.003	5.05	42.08
Bayerite	2.5	1.00	0.007	2.97	2.97
Gibbsite	4.1	0.61	0.009	1.67	2.74

[a]$q_{max,m}$ and $q_{max,s}$ represent the maximum defluoridation capacity per unit mass and area, respectively.

Table 4 | Adsorption capacities of different Al-based adsorbents for fluoride removal from water

Adsorbents	C_0 (mg L^{-1})	pH	Contact time (h)	q_{max} (mg g^{-1})	References
Al_2O_3 modified expanded graphite	3–100	4.0	2.5	5.75	Jin *et al.* (2015)
Mesoporous $CoAl_2O_4$	5–50	7.0	5	14.80	Zhao *et al.* (2015)
$Al(OH)_3$ modified magnetite	1–30	7.8	24	1.51	García-Sánchez *et al.* (2016)
Bayerite/boehmite	10–100	7.0	24	56.80	Jia *et al.* (2015a, 2015b)
Sulfate modified AlOOH	20–100	6.0	24	40.0	Du *et al.* (2014)
Activated Al_2O_3	2.5–14	7	24	1.45	Ghorai & Pant (2004)
Al_2O_3 cement granule	2.5–100	6.5–7	3	10.21	Ayoob & Gupta (2008)
α-Al_2O_3	3–10	5	24	2.73	Valdivieso *et al.* (2006)
γ-Al_2O_3	1–100	6.15	24	14.0	Kumar *et al.* (2011)
Al_2O_3 nanoparticles	1–50	5–6	2	9.73	Tangsir *et al.* (2016)
Mesoporous Al_2O_3	20–250	6	24	14.26	Lee *et al.* (2010)
Gibbsite	10–40	7.5	12	1.67	This study
Bayerite	10–40	7.5	12	2.97	This study
Boehmite	10–40	7.5	12	5.05	This study

Physicochemical mechanism

It is significant to comprehend the fluoride removal mechanisms, which is helpful to analyze the difference in defluoridation performance of different aluminum hydroxides. As is known, there is a layer of hydroxyl groups on the surfaces of aluminum hydroxide. Moreover, aluminum hydroxide has a stronger affinity for fluoride than the hydroxyl group (Pommerenk & Schafran 2005). Therefore, when the aluminum hydroxide is put into F^- solution, the surface hydroxyl groups can exchange with F^-

$$F^- + \equiv AlOH \leftrightarrow \equiv AlF + OH^- \quad (6)$$

where $\equiv AlOH$ represents the hydroxyl groups on aluminum hydroxide surfaces. After reaction, fluoride adsorbs on the adsorbent surface, and OH^- is released into aqueous solution. In this case, the pH value of the solution will slightly increase.

To confirm the above fluoride removal mechanism, the pH values before and after fluoride removal by different aluminum hydroxides were measured and are shown in Table 5. For all the aluminum hydroxides, the pH values increase after fluoride removal. Furthermore, the higher the defluoridation efficiency, the larger the change in pH value (ΔpH) becomes. When defluoridation efficiency increases, more F^- adsorbs on aluminum hydroxide, resulting in the release of more OH^-. This confirms the above fluoride removal mechanism.

Figure 9 demonstrates the FTIR spectra of boehmite before and after adsorption. It can be seen that the peak of 1,384 cm^{-1} belonging to the surface hydroxyl groups obviously decreases after fluoride adsorption (Xu *et al.* 2015), meaning that surface hydroxyl groups are involved in the fluoride adsorption process. This validates that the exchange between surface hydroxyl groups and fluoride is the main mechanism for fluoride adsorption on aluminum hydroxide.

Table 5 | pH values of different solutions before and after fluoride removal by different aluminum hydroxides

Adsorbents[a]	pH (before)	pH (after)	ΔpH
Gibbsite	7.72	7.89	0.17
Bayerite	7.72	8.01	0.29
Boehmite	7.49	7.94	0.45

[a]The initial fluoride concentration of solution is 20 mg/L.

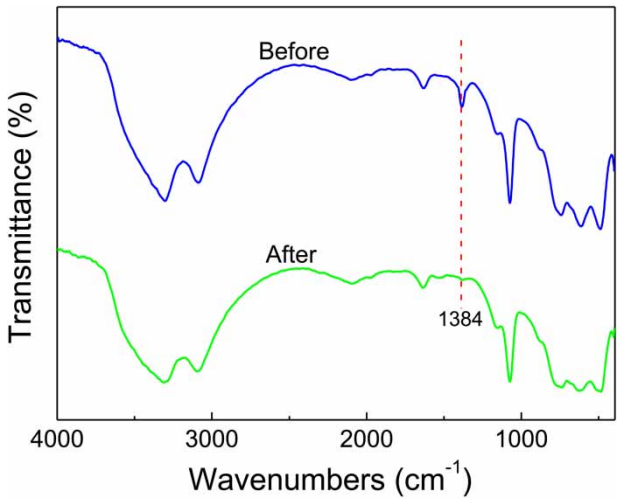

Figure 9 | FTIR spectra of boehmite adsorbent before and after fluoride removal from aqueous solution with initial F^- concentration of 40 mg L^{-1}.

Based on the above analyses, it can be concluded that the defluoridation capacity of aluminum hydroxide greatly depends on its surface hydroxyl group density. In fact, the surface hydroxyl group density of aluminum hydroxide varies with the crystalline phase. The surface hydroxyl group density of boehmite, bayerite and gibbsite is 16.5, 12.0 and 8.0 sites nm^{-2}, respectively (Sposito 1996; Lefèvre *et al.* 2002; Karamalidis & Dzombak 2010). This may be the reason why the defluoridation capacities of different aluminum hydroxides follow the order of boehmite > bayerite > gibbsite.

CONCLUSIONS

In this research, the defluoridation performances of aluminum hydroxides with different crystalline phases are compared and evaluated in terms of fluoride removal capacity, sensitivity to pH values and residual Al concentration after defluoridation. The results indicated that the defluoridation performances of different aluminum hydroxides follow the order of boehmite > bayerite > gibbsite. For boehmite, it can remove >60% fluoride in the first 1.5 h, and reach adsorption equilibrium within 12 h. The maximum defluoridation capacities of boehmite, bayerite and gibbsite based on Langmuir isotherm model are 42.08, 2.97 and 2.74 mg m^{-2}. The pH values and FTIR analyses reveal that the fluoride removal is mainly attributed to the ligand exchange between fluoride and surface hydroxyl groups. Different aluminum hydroxides have different surface hydroxyl group density, which results in the different defluoridation capacity. This work provides a new idea for the preparation of aluminum hydroxide with excellent adsorption performance.

ACKNOWLEDGEMENTS

This work is supported by the National Natural Science Foundation of China (Grant Nos. 51872181 and 51801093), the Key scientific research projects of Henan Province Colleges and Universities (No. 22A480006), and the Youth Backbone Teacher of Henan Province (No. 2020GGJS197).

DATA AVAILABILITY STATEMENT

All relevant data are included in the paper or its Supplementary Information.

REFERENCES

Alex, T. C., Kumar, R., Roy, S. K. & Mehrotra, S. P. 2014 Mechanically induced reactivity of gibbsite: part1. Planetary milling. *Powder Technology* **264**, 105–113.

Alkurdi, S. S. A., Al-Juboori, R. A., Bundschuh, J. & Hamawand, I. 2019 Bone char as a Green sorbent for removing health threatening fluoride from drinking water. *Environment International* **127**, 704–719.

Ayoob, S. & Gupta, A. K. 2008 Insights into isotherm making in the sorptive removal of fluoride from drinking water. *Journal of Hazardous Materials* **152**, 976–985.

Dayananda, D., Sarva, V. R., Prasad, S. V., Arunachalam, J., Parameswaran, P. & Ghosh, N. N. 2015 Synthesis of MgO nanoparticle loaded mesoporous Al_2O_3 and its defluoridation study. *Applied Surface Science* **329**, 1–10.

Du, J. Y., Sabatini, D. A. & Butler, E. C. 2014 Synthesis, characterization, and evaluation of simple aluminum-based adsorbents for fluoride removal from drinking water. *Chemosphere* **101**, 21–27.

Gai, W. Z. & Deng, Z. Y. 2021 A comprehensive review of adsorbents for fluoride removal from water: performance, water quality assessment and mechanism. *Environmental Science: Water Research & Technology* **7** (8), 1362–1386.

Gai, W. Z., Deng, Z. Y. & Shi, Y. 2015 Fluoride removal from water using high-activity aluminum hydroxide prepared by the ultrasonic method. *Rsc Advances* **5** (102), 84223–84231.

García-Sánchez, J. J., Solache-Ríos, M., Martínez-Gutiérerez, J. M., Arteaga-Larios, N. V., Ojeda-Escamilla, M. C. & Rodríguez-Torres, I. 2016 Modified natural magnetite with Al and La ions for the adsorption of fluoride ions from aqueous solutions. *Journal of Fluorine Chemistry* **186**, 115–124.

George, S., Pandit, P. & Gupta, A. B. 2010 Residual aluminum in water defluoridated using activated alumina adsorption – modeling and simulation studies. *Water Research* **44** (10), 3055–3064.

Ghorai, S. & Pant, K. K. 2004 Investigations on the column performance of fluoride adsorption by activated alumina in a fixed-bed. *Chemical Engineering Journal* **98** (1–2), 165–173.

He, Y. X., Zhang, L. M., An, X., Wan, G. P., Zhu, W. J. & Luo, Y. M. 2019 Enhanced fluoride removal from water by rare earth (La and Ce) modified alumina: adsorption isotherms, kinetics, thermodynamics and mechanism. *Science of Total Environment* **688**, 184–198.

He, J. Y., Yang, Y., Wu, Z. J., Xie, C., Zhang, K. S., Kong, L. T. & Liu, J. H. 2020 Review of fluoride removal from water environment by adsorption. *Journal of Environmental Chemical Engineering* **8** (6), 104516.

Hegde, R. M., Rego, R. M., Potla, K. M., Kurkuri, M. D. & Kigga, M. 2020 Bio-inspired materials for defluoridation of water: a review. *Chemosphere* **253**, 126657.

Jia, Y., Zhu, B. S., Jin, Z., Sun, B., Luo, T., Yu, X. Y., Kong, L. T. & Liu, J. H. 2015a Fluoride removal mechanism of bayerite/boehmite nanocomposites: roles of the surface hydroxyl groups and the nitrate anions. *Journal of Colloid and Interface Science* **440**, 60–67.

Jia, Y., Zhu, B. S., Zhang, K. S., Jin, Z., Sun, B., Luo, T., Yu, X. Y., Kong, L. T. & Liu, J. H. 2015b Porous 2-line ferrihydrite/bayerite composites (LFBC): fluoride removal performance and mechanism. *Chemical Engineering Journal* **268**, 325–336.

Jin, H. Y., Ji, Z. J., Yuan, J., Li, J., Liu, M., Xu, C. H., Dong, J., Hou, P. & Hou, S. 2015 Research on removal of fluoride in aqueous solution by alumina-modified expanded graphite composite. *Journal of Alloys and Compounds* **620**, 361–367.

Kameda, T., Oba, J. & Yoshioka, T. 2015 Recyclable Mg-Al layered double hydroxides for fluoride removal: kinetic and equilibrium studies. *Journal of Hazardous Materials* **300**, 475–482.

Karamalidis, A. K. & Dzombak, D. A. 2010 *Surface Complexation Modeling: Gibbsite*. John Wiley & Sons, Pennsylvania, New Jersey.

Kumar, E., Bhatnagar, A., Kumar, U. & Sillanpää, M. 2011 Defluoridation from aqueous solutions by nano-alumina: characterization and sorption studies. *Journal of Hazardous Materials* **186**, 1042–1049.

Lee, G., Chen, C., Yang, S. T. & Ahm, W. S. 2010 Enhanced adsorptive removal of fluoride using mesoporous alumina. *Microporous Mesoporous Materials* **127**, 152–156.

Lefèvre, G., Duc, M., Lepeut, P., Caplain, R. & Fédoroff, M. 2002 Hydration of γ-alumina in water and its effects on surface reactivity. *Langmuir* **18** (20), 7530–7537.

Musić, S., Dragĉević, D., Popović, S. & Vdović, N. 1999 Chemical and microstructural properties of Al-oxide phases obtained from $AlCl_3$ solutions in alkaline medium. *Materials Chemistry Physics* **59** (1), 12–19.

Pommerenk, P. & Schafran, G. C. 2005 Adsorption of inorganic and organic ligands onto hydrous aluminum oxide: evaluation of surface charge and the impacts on particle and NOM removal during water treatment. *Environmental Science & Technology* **39** (17), 6429–6434.

Rondeau, V., Commenges, D., Gadda, H. J. & Dartigues, J. F. 2000 Relation between aluminum concentrations in drinking water and Alzheimer's disease: an 8-year follow-up study. *American Journal of Epidemiology* **152** (1), 59–66.

Shimelis, B., Zewge, F. & Chandravanshi, B. S. 2006 Removal of excess fluoride from water by aluminum hydroxide. *Bulletin of the Chemical Society of Ethiopia* **20** (1), 17–34.

Sposito, G. 1996 *Environmental Chemistry of Aluminum*. CRC Press, California.

Srivastav, A. L., Singh, P. K., Srivastava, V. & Sharma, Y. C. 2013 Application of a new adsorbent for fluoride removal from aqueous solutions. *Journal of Hazardous Materials* **263**, 342–352.

Sun, R. H., Zhang, H. B., Qu, J., Yao, H., Yao, J. & Yu, Z. Z. 2016 Supercritical carbon dioxide fluid assisted synthesis of hierarchical AlOOH@reduced graphene oxide hybrids for efficient removal of fluoride ions. *Chemical Engineering Journal* **292**, 174–182.

Tangsir, S., Hafshejani, L. D., Lähde, A., Maljanen, M., Hooshman, A., Naseri, A. A., Moazed, H., Jokiniemi, J. & Bhatnagar, A. 2016 Water defluoridation using Al_2O_3 nanoparticles synthesized by flame spray pyrolysis (FSP) method. *Chemical Engineering Journal* **288**, 198–206.

Valdivieso, A. L., Bahena, J. L. R., Song, S. & Urbina, R. H. 2006 Temperature effect on the zeta potential and fluoride adsorption at the α-Al_2O_3/aqueous solution interface. *Journal of Colloid and Interface Science* **298** (1), 1–5.

Wang, S. G., Ma, Y., Shi, Y. J. & Gong, W. X. 2009 Defluoridation performance and mechanism of nano-scale aluminum oxide hydroxide in aqueous solution. *Journal of Chemical Technology and Biotechnology* **84** (7), 1043–1050.

Xie, D. H., Gu, Y., Wang, H. J., Wang, Y. C., Qin, W. X., Wang, G. Z., Zhang, H. M. & Zhang, Y. X. 2019 Enhanced fluoride removal by hierarchically porous carbon foam monolith with high loading of UiO-66. *Journal of Colloid Interface Science* **542**, 269–280.

Xu, Z. H., Yu, J. G. & Jaroniec, M. 2015 Efficient catalytic removal of formaldehyde at room temperature using AlOOH nanoflakes with deposited Pt. *Applied Catalysis B Environmental* **163**, 306–312.

Zhang, Y. Z. & Huang, K. 2019 Grape pomace as a biosorbent for fluoride removal from groundwater. *RSC Advances* **9** (14), 7767–7776.

Zhang, H. L., Li, P., Cui, W. W., Liu, C., Wang, S. L., Zheng, S. L. & Zhang, Y. 2016 Synthesis of nanostructured γ-AlOOH and its accelerating behavior on the thermal decomposition of AP. *Rsc Advances* **6** (32), 27235–27241.

Zhao, X., Zhang, L. M., Xiong, P., Ma, W. J., Qian, N. & Lu, W. C. 2015 A novel method for synthesis of Co-Al layered double hydroxides and their conversions to mesoporous $CoAl_2O_4$ nanostructures for applications in adsorption removal of fluoride ions. *Microporous and Mesoporous Materials* **201**, 91–98.

First received 12 May 2021; accepted in revised form 2 January 2022. Available online 11 January 2022